

. SCUOLA INTERNAZIONALE SUPERIORE DI STUDI AVANZATI

SISSA Digital Library

Templated growth of metal-organic coordination chains at surfaces

Original
Templated growth of metal-organic coordination chains at surfaces / Classen, T., Fratesi, G., Costantini, G., Fabris, S., Stadler, F.L., Kim, C., de Gironcoli, S., Baroni, S., Kern, K.. - In: ANGEWANDTE CHEMIE. INTERNATIONAL EDITION. - ISSN 1433-7851. - 44:38(2005), pp. 6142-6145. [10.1002/anie.200502007]

Availability:
This version is available at: 20.500.11767/16126 since:

Publisher:

Published
DOI:10.1002/anie.200502007

Terms of use:

Testo definito dall'ateneo relativo alle clausole di concessione d'uso

Publisher copyright

note finali coverpage

(Article begins on next page)

21 November 2026

Templated Growth of Metal-Organic Coordination Chains at Surfaces **

*Thomas Classen *, Guido Fratesi, Giovanni Costantini, Stefano Fabris *, Frank Louis Stadler, Cheolkyu Kim, Stefano de Gironcoli, Stefano Baroni, Klaus Kern **

Metal-organic coordination networks (MOCNs) formed by coordination bonding between metallic centers and organic ligands can be efficiently engineered to exhibit specific magnetic, electronic, or catalytic properties. [1–6] Instead of depositing prefabricated MOCNs onto surfaces, it has been recently shown that two dimensional (2D) MOCNs can be directly grown at metal surfaces in ultra high vacuum (UHV), thus creating highly regular 2D networks of metal atoms. [7–12] These grids have been pointed out to be potentially relevant for devices involving sensing, switching, and information storage. [13,14] We show here that this approach offers the additional advantage to predefine the MOCN geometry by using the substrate as template to direct the formation of novel 1D metal-organic coordination chains (MOCCs).

The templating role of substrates is well known in the field of surface epitaxial growth. [15–19] Among the highly anisotropic substrates, the Cu(110) surface is one of the most common (Figure 1a and b). In order to evidence its strong 1D templating effect on organic molecules, a ligand with a triangular symmetry was selected: 1,3,5-benzenetricarboxylic acid (trimesic acid, TMA, Figure 1c). In fact, the 3-fold rotation symmetry supports the formation of hexagonal 2D and 3D architectures, [20–22] therefore strongly disfavoring the linear geometry. On the isotropic Cu(100) surface, TMA forms 0D carboxylate complexes and 2D networks. [9,10]

The UHV deposition of TMA on Cu(110) at 300 K results in the formation of 1D chains along the $\langle 1\bar{1}0 \rangle$ direction, as observed by STM. This deposition temperature is high enough to

**The authors wish to acknowledge Nian Lin, Magalí Lingenfelder, Alexander Schneider and Giacinto Scoles for fruitful discussions, HPC-EUROPA (project #506079) and INFM Progetto Calcolo Parallelo for computer resources.

*T. Classen, Dr. G. Costantini, Dr. F. L. Stadler, Dr. C. Kim, Prof. K. Kern
Max-Planck-Institut für Festkörperforschung
Heisenbergstr. 1, 70569 Stuttgart (Germany)
Fax: (+49) 711-689-1662
Email: t.classen@fkf.mpg.de, k.kern@fkf.mpg.de
G. Fratesi, Dr. S. Fabris, Prof. S. de Gironcoli, Prof. S. Baroni
SISSA and INFM-CNR DEMOCRITOS National Simulation Center
Via Beirut 2-4, I-34014 Trieste (Italy)
E-mail: fabris@democritos.it

provide mobile Cu adatoms via evaporation from kinks and steps onto the terraces. [23] These adatoms have been found by XPS analysis for similar systems to catalyze the deprotonation of the molecular carboxylic groups, [24,25] and are furthermore necessary for the formation of Cu carboxylate complexes. [23,24,26] Depositing at lower temperatures, 210 K and 250 K, resulted in disordered structures with a tip to tip bonding motif. This signature which is never observed above 300 K is characteristic for intramolecular dimeric hydrogen bonds of carboxylic groups, [20–22,24] thus indicating that the carboxylic groups are protonated for temperatures below 300 K. Annealing to 300 K of these structures yields to the same 1D chains described above. The 300 K chains typically show irregular kinks and poor long-range order. These inhomogeneities are lifted by a post-annealing to 380-410 K, yielding straight and highly periodic chains, referenced MOCC-I hereafter (Figure 2). At low coverage, chains predominantly attach to step edges, while by increasing the coverage chain nucleation takes place also on terraces.

These findings allow to rationalize the substrate templating effect as follows: Upon deprotonation, the molecule-molecule interaction (favoring hexagonal geometries) is overcome by the molecule-substrate interaction, which effectively controls the 1D character of these MOCCs.

The chains consist of triangles alternating with round protrusions (Figure 2b and c). The apparent height of the two units is significantly different: 140 ± 30 pm and 75 ± 20 pm, respectively, when scanning at -1 V and 1 nA. Following previous analysis, [9,10,20–22] the triangles are identified as flat-lying TMA molecules. The round protrusions can be attributed to Cu adatoms, [7,9,10] coordinated by two of the carboxylate groups of the TMA molecule. The third TMA functional group is pointing out of the chain with no preferential up or down orientation (Figure 2b).

The periodicity of the MOCC-I along $\langle 1\bar{1}0 \rangle$ is 5 Cu lattice spacings (12.70 ± 0.15 Å). High-resolution STM images indicate that the distance between the Cu-protrusion and the O atom of the molecular carboxylate groups is ≈ 2.8 Å, a rather large value when compared to the typical Cu-O bond length of 1.9-2.2 Å. [27] The simplest [-TMA-Cu-]$_n$ chain model for the MOCC-I adsorption geometry seems therefore to be outruled by these observations.

Indeed, the lowest energy MOCC-I structure predicted by density functional theory (DFT) calculations is a [-Cu-TMA-Cu-]$_n$ chain in which a dimer of Cu metal adatoms forms uniden-

tate Cu carboxylate bonds with adjacent TMA molecules (Figure 2d). The dimer binds to the surface by 6.3 eV and each adatom is 5-fold coordinated to the substrate. This structure has the right 5× periodicity. Its simulated STM image (Figure 2e) closely agrees with the experimental one, the Cu-Cu dimer being imaged as a single spot centered between the adatoms. The resulting Cu-O distance is 2.02 Å, therefore in the range of the typical Cu-O bond lengths. Finally, also the calculated apparent heights, 170 pm for the TMA and 90 pm for the Cu-protrusion, are in good agreement with the experimental ones.

The theoretical analysis provides an unprecedented level of insight into the adsorbtion geometry of surface MOCNs. The TMA phenyl ring and the Cu adatoms are located on the short-bridge and hollow sites, respectively (Figure 2d). The molecule stands 1.14 Å above the outermost Cu layer, the carboxylate groups bending towards the surface by as much as 0.69 Å. With respect to a neutral Cu atom, surface Cu-complexation weakly reduces the metal center occupations of both the s and d electronic states by ≈ 0.2 electrons.

[-Cu-TMA-Cu-]$_n$ chains are the intrinsic nanostructures on Cu(110), but functional MOCCs require also different elements than Cu as metallic centers. Extrinsic [-TMA-Fe-]$_n$ chains (MOCC-II) were created by holding the Cu(110) crystal at 230 K – thus preventing the formation of Cu-TMA complexes – and by depositing first TMA and then Fe at coverages higher than 0.04 ML. The sample was then annealed to 390 K for one minute. The number of chains increased with the amount of deposited Fe and saturation was reached for a coverage of ≈ 0.08 ML of Fe. Further Fe deposition results in the nucleation of Fe islands.

The 4× in-chain periodicity of these chains (Figure 3) leaves space for just one Fe metal center between TMAs. The TMA-TMA distances are therefore shorter when linked by Fe than when linked by Cu, similarly to what was reported for 2D MOCN on the Cu(001) surface. [9, 10] According to DFT calculations, the geometry of the adsorbed TMA molecule is weakly dependent on the metal center: the phenyl ring being 0.09 Å higher in the case of Fe. The metal-carboxylate bond is still unidentate and the Fe-O distance is 1.95 Å thus 0.07 Å shorter than the Cu-O one in MOCC-I. Single metal centers lead to very weak features in the simulated STM image (Figure 3d), in agreement with experiment (Figure 3b). With respect to a neutral Fe atom, surface Fe-complexation strongly reduces the occupations of the Fe-s states by 1.3 electrons while increases that of the d states by 0.5 electrons.

Insight into the potentially interesting magnetic properties of these Fe-complexated MOCC-

II can be gained by projecting the electron density on the atomic Fe-*d* orbitals (Figure 4b). The projected density of electronic states (DOS) displays a large splitting between the majority *spin-up* and minority *spin-down* electron *d*-states. The former are completely filled and well hybridized with the substrate Cu *d*-states, extending from -5 to -1 eV in the total DOS of the [-TMA-Fe-]$_n$ chain (Figure 4a). The latter are only partially filled and extend in the energy region dominated by the substrate *s*-states. As a consequence, the Fe atoms are strongly magnetized, with a spin polarization of 3.3 μ_B per Fe atom. The polarization of a Fe adatom isolated on the Cu(110) surface is very similar, 3.2 μ_B, and the corresponding projected DOS is shown in Figure 4c. The comparison shows that isolated Fe-adatoms and carboxylated Fe centers exhibit very similar magnetic properties, which are evidently not strongly influenced by the presence of the molecular linkers.

In particular, the coordination with the carboxylate group does not affect the electron localization at the Fe adatoms, thus not producing any relevant quenching of the spin magnetic moment. This is a necessary (although not sufficient) condition for the emergence of intriguing magnetic properties induced by the low dimensionality, such as giant magnetic anisotropy. [28,29] Because of their high thermal stability, MOCNs similar to those presented here could thus be convenient model systems where to explore the occurrence of low-dimensional magnetism.

In conclusion, metal-organic coordination chains were created in situ by self-organized growth at a metal surface in UHV. The 1D anisotropy of the substrate was effectively transferred to the resulting metal-organic coordination chains. This strategy was shown to work for intrinsic as well as for extrinsic metal-carboxylate systems. The precise atomic configuration of the structures was revealed by a combined use of STM and DFT. Spin-polarized DFT suggests that Fe centers within the 1D chains have magnetic properties similar to those of isolated Fe adatoms. This renders such regular and unidirectional arrangement of magnetic centers attractive candidates for the investigation of low-dimensional magnetism in thermally stable structures.

Methods

The sample was prepared in a standard UHV preparation-chamber with a base pressure of less than $2 \cdot 10^{-10}$ mbar. The Cu(110) single crystal was cleaned by cycles of Ar^+-sputtering (900 eV) and annealing to 830 - 850 K. Commercially available TMA (Fluka Chemie AG, purity $> 97\%$) was evapo-

rated from a ceramic crucible at 460 K for sample temperatures between 130 K and 300 K. The sample was then transferred under UHV-conditions to a STM-chamber (base pressure of $6 \cdot 10^{-11}$ mbar) comprising a commercial variable temperature STM. Measurements were carried out at 300 K and at 130 K with typical tunnelling conditions of -1 V and 1 nA (filled state imaging).

The computer simulations were based on DFT, in the generalized gradient approximation of Perdew-Burke-Ernzerhof. [30] The calculations were performed in the pseudopotential plane-wave framework (plane wave cutoff of 326.4 eV) using ultra-soft pseudopotentials [31] as implemented in the PWscf simulation package. [32] A 3-layer slab provided a simplified model of the Cu (110) surface. The atomic positions were determined by relaxing the upper layer and keeping the distance between the others fixed at the bulk value. Metal adatoms and deprotonated TMA molecules were positioned on the upper surface of the slab and were structurally relaxed according to the Hellmann-Feynman forces. STM images were simulated by means of the Tersoff-Hamann method, [33] *i.e.* by a spatially resolved DOS integrated in energy from a bias potential (-1.0 eV) to the Fermi energy.

References

[1] O. M. Yaghi, M. O'Keeffe, N. W. Ockwig, H. K. Chae, M. Eddaoudi, J. Kim. *Nature* **2003**, *423*, 705.

[2] G F. Swiegers, T. J. Malefetse. *Chem. Rev.* **2000**, *100*, 3483.

[3] B. J. Holliday, C. A. Mirkin. *Angew. Chem.* **2001**, *113*, 2076; *Angew. Chem. Int. Ed.* **2001**, *40*, 2022

[4] C. Copéret, M. Chabanas, R. P. Saint-Arroman, J.-M. Basset. *Angew. Chem.* **2003**, *115*, 164; *Angew. Chem. Int. Ed.* **2003**, *42*, 156.

[5] C. Nozaki, C. G. Lugmair, A. T. Bell, T. Don Tilley. *J. Am. Chem. Soc.* **2002**, *124*, 13194.

[6] H. Srikanth, R. Hajndl, B. Moulton, M. J. Zaworotko. *J. Appl. Phys.* **2003**, *93*, 7089.

[7] A. Dmitriev, H. Spillmann, N. Lin, J. V. Barth, K. Kern. *Angew. Chem.* **2003**, *115*, 2774; *Angew. Chem. Int. Ed.* **2003**, *42*, 2670; S. Stepanow, M. Lingenfelder, A. Dmitriev, H. Spillmann, E. Delvigne, N. Lin, X. Deng, C. Cai, J. V. Barth, K. Kern. *Nature Mat.* **2004**, *3*, 229.

[8] D. G. Kurth, N. Severin, J. P. Rabe. *Angew. Chem.* **2002**, *114*, 3833; *Angew. Chem. Int. Ed.* **2002**, *41*, 3681.

[9] N. Lin, A. Dmitriev, J. Weckesser, J. V. Barth, K. Kern. *Angew. Chem.* **2002**, *114*, 4973; *Angew. Chem. Int. Ed.* **2002**, *41*, 4779.

[10] P. Messina, A. Dmitriev, N. Lin, H. Spillmann, M. Abel, J. V. Barth, K. Kern. *J. Am. Chem. Soc.* **2002**, *124*, 14000.

[11] S. De Feyter, M. M. S. Abdel-Mottaleb, N. Schuurmans, B. J. V. Verkuijl, J. H. van Esch, B. L. Feringa, F. C. De Schryver. *Chem. Eur. J.* **2004**, *10*, 1124.

[12] M. Ruben. *Angew. Chem.* **2005**, *117*, 1620; *Angew. Chem. Int. Ed.* **2005**, *44*, 1594.

[13] J.-M. Lehn. *Supramolecular chemistry*, VCH, Weinheim **1995**, chapter 9, p. 200.

[14] M. Ruben, J. Rojo, F. J. Romero-Salguero, L. H. Uppadine, J.-M. Lehn. *Angew. Chem.* **2004**, *116*, 3728; *Angew. Chem. Int. Ed.* **2004**, *43*, 3644.

[15] H. Röder, E. Hahn, H. Brune, J.-P. Bucher, K. Kern. *Nature* **1993**, *366*, 141.

[16] S. Lukas, G. Witte, C. Wöll. *Phys. Rev. Lett.* **2002**, *88*, 028301.

[17] A. Kühnle, L. M. Molina, T. R. Linderoth, B. Hammer, F. Besenbacher. *Phys. Rev. Lett.* **2004**, *93*, 086101.

[18] P. Gambardella, M. Blanc, H. Brune, K. Kuhnke, K. Kern. *Phys. Rev. B* **2000**, *61*, 2254.

[19] P. W. Murray, I. M. Brookes, S. A. Haycock, G. Thornton. *Phys. Rev. Lett.* **1998**, *80*, 988.

[20] S. Griessl, M. Lackinger, M. Edelwirth, M. Hietschold, W. M. Heckl. *Single Mol.* **2002**, *3*, 25.

[21] Y. Ishikawa, A. Ohira, M. Sakata, C. Hirayama, M. Kunitake. *Chem. Commun.* **2002**, *22*, 2652.

[22] G.-J. Su, H.-M. Zhang, L.-J. Wan, C.-L. Bai, T. Wandlowski. *J. Phys. Chem. B* **2004**, *108*, 1931.

[23] C. C. Perry, S. Haq, B. G. Frederick, N. V. Richardson. *Surf. Sci* **1998**, *409*, 512.

[24] N. Lin, D. Payer, A. Dmitriev, T. Strunskus, C. Wöll, J.V. Barth, K. Kern. *Angew. Chem.* **2005**, *117*, 1512; *Angew. Chem. Int. Ed.* **2005**, *44*, 1488.

[25] S. Stepanow, T. Strunskus, M. Lingenfelder, A. Dmitriev, H. Spillmann, N. Lin, J. V. Barth, Ch. Wöll, K. Kern *J. Phys. Chem. B* **2004**, *108*, 19392.

[26] D. S. Martin, R. J. Cole, S. Haq. *Phys. Rev. B* **2002**, *66*, 155427.

[27] A. Doyle, J. Felcman, M. T. do Prado Gambardella, C. N. Verani, M. L. Bragança Tristão. *Polyhedron* **2000**, *19*, 2621.

[28] P. Gambardella, A. Dallmeyer, K. Maiti, M. C. Malagoli, W. Eberhardt, K. Kern, C. Carbone. *Nature* **2002**, *416*, 301.

[29] P. Gambardella, S. Rusponi, M. Veronese, S. S. Dhesi, C. Grazioli, A. Dallmeyer, I. Cabria, R. Zeller, P. H. Dederichs, K. Kern, C. Carbone, H. Brune. *Science* **2003**, *300*, 1130.

[30] J. P. Perdew, K. Burke, M. Ernzerhof. *Phys. Rev. Lett.* **1996**, *77*, 3865.

[31] D. Vanderbilt. *Phys. Rev. B* **1990**, *41*, 7892.

[32] S. Baroni, A. Dal Corso, S. de Gironcoli, P. Giannozzi. `http://www.pwscf.org`.

[33] J. Tersoff, D. R. Hamann. *Phys. Rev. Lett.* **1983**, *50*, 1998.

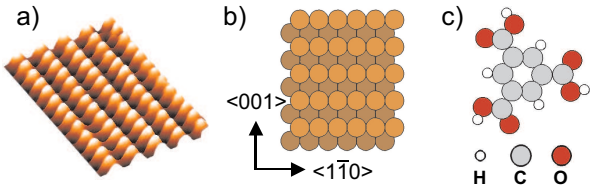


Figure 1: a) High resolution STM image in 3D representation and b) structural model of the Cu(110) surface. c) trimesic acid (TMA).

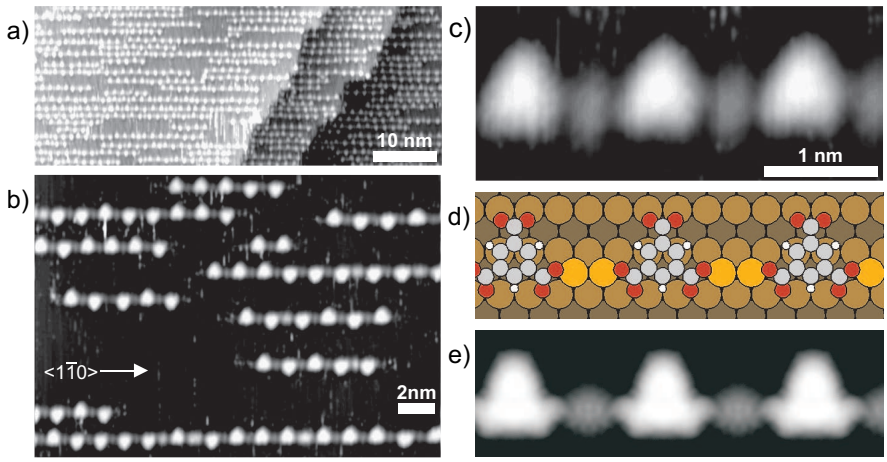


Figure 2: STM representative images of [-Cu-TMA-Cu-]$_n$ chains (MOCC-I) on Cu(110) for TMA coverages of a) 0.36 and b) 0.13 monolayer (ML), respectively. Comparison of c) the high resolution STM image of MOCC-I, d) the atomistic MOCC-I model, and e) the corresponding simulated STM image.

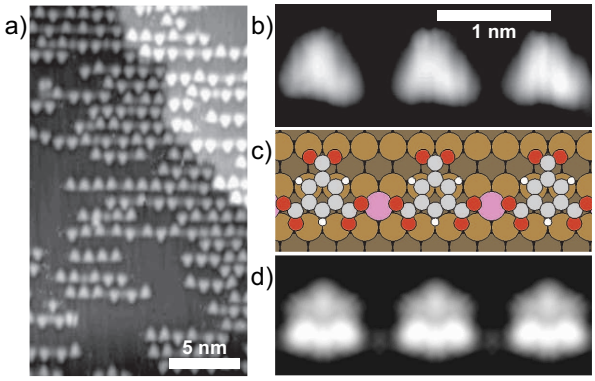


Figure 3: [-TMA-Fe-]$_n$ chains (MOCC-II): a) Overview image of the coordination chains formed upon deposition of 0.04 ML Fe and 0.40 ML TMA. Comparison of b) the high resolution STM image , c) the atomistic MOCC-II model, and d) the corresponding simulated STM image.

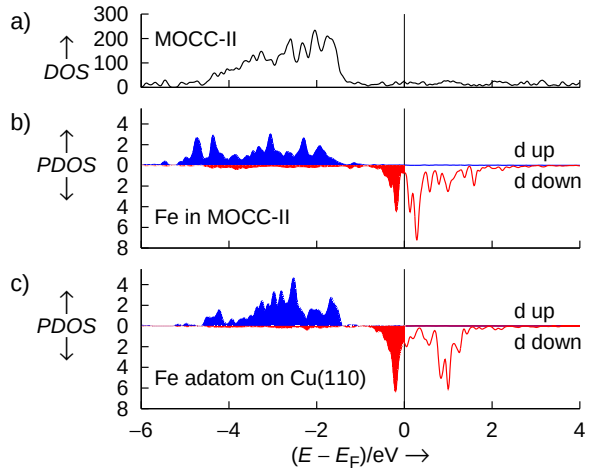
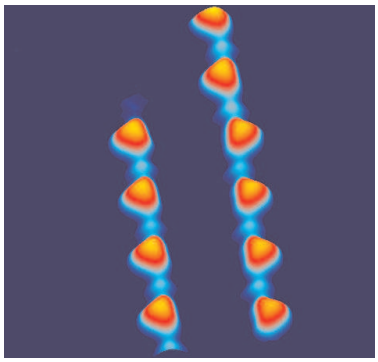


Figure 4: a) Total DOS (in states/eV with respect to the Fermi energy E_F) of the [-TMA-Fe-]$_n$ chain (MOCC-II), and projected DOS (PDOS) on the atomic d-states of b) the Fe center in the MOCC-II and c) a Fe atom isolated on the Cu(110) surface.



Line up, please

Highly anisotropic metal surfaces can drive the formation of metal-organic coordination chains, as shown by a combined STM and DFT analysis. These 1D arrangements of metal centers (Fe, Cu) regularly spaced by organic linkers open new possibilities for the study of low-dimensional magnetism.

T. Classen, G. Fratesi, G. Costantini, S. Fabris, F. L. Stadler, C. Kim, S. de Gironcoli, S. Baroni, K. Kern

Templated Growth of Metal-Organic Coordination Chains at Surfaces

Keywords

Self-assembly

Scanning probe microscopy

Density functional calculations

Nanomaterials

Coordination compounds